Organic Electronics 14 (2013) 1629–1635

Contents lists available at SciVerse ScienceDirect

Organic Electronics

journal homepage: www.elsevier.com/locate/orgel

Enhanced performance in inverted polymer solar cells via solution process: Morphology controlling of PEDOT:PSS as anode buffer layer by adding surfactants

Soo Won Heo, Kyeong Hoon Baek, Tae Ho Lee, Joo Young Lee, Doo Kyung Moon *

Department of Materials Chemistry and Engineering, Konkuk University, 1 Hwayang-dong, Gwangjin-gu, Seoul 143-701, Republic of Korea

ARTICLE INFO

Article history:
Received 25 January 2013
Received in revised form 26 March 2013
Accepted 27 March 2013
Available online 9 April 2013

Keywords:
Inverted polymer solar cells
Buffer layer
PEDOT:PSS
Surfactant
Stability

ABSTRACT

Inverted polymer solar cells were fabricated by adding the amphiphilic surfactant 'Surfynol 104 series' to Poly(3,4-ethylenedioxythiophene):poly(styrenesulfonate) (PEDOT:PSS) as a anode buffer layer by solution process. With the introduction of Surfynol 104 series-added PEDOT:PSS, it was able to form a homogeneous film by adjusting the wettability of a hydrophobic poly(3-hexylthiophene) (P3HT):[6,6]-phenyl C_{61}-butyric acid methyl ester (PCBM) film. With decrease in series resistance (R_S) and increase in shunt resistance (R_{SH}), as a result, the short circuit current density (J_{SC}), open circuit voltage (V_{OC}) and fill factor (FF) of the optimized device were 10.2 mA/cm^2, 0.63 V and 61.3%, respectively, calculated the power conversion efficiency (PCE) was 4.0%. In addition, the air stability of the fabricated device was improved.

1. Introduction

Polymer–fullerene bulk heterojunction solar cells (BHJ PSCs) have been praised as renewable, lightweight and low-cost energy sources [1–5]. They are now over 8% in terms of power conversion efficiency (PCE) [6,7]. To enhance the PCE of PSCs, there have been studies on the synthesis of new narrow band gap materials for better photon harvesting, optimization of phase segregation in the bulk heterojunction (BHJ) layers, interfacial modification for better charge carrier collection and design of novel configuration cells [8–13].

For commercialization of BHJ PSCs, stability as well as PCE should be enhanced. The conventional BHJ PSCs have sandwich structure with a photo-active layer between two electrodes, having a high-work function transparent metal oxide as bottom anode and a low-work function metal as top cathode. For efficient charge collection, therefore, the work function of anode and cathode should be well matched with the highest occupied molecular orbits (HOMOs) level of donor materials and lowest unoccupied molecular orbits (LUMOs) level of acceptor materials. Top cathode usually uses a low-work function metal for matching with the LUMO level of acceptors. However, they have low long-term stability because they are very sensitive to oxygen and moisture in the air [14,15]. To avoid this kind of problem, bi-layer (Ca/Al, Ba/Al, etc.)-structured cathodes were introduced. However, this method requires a complete encapsulation process to block oxygen and moisture.

Recently, therefore, there have been extensive investigations of PSCs with an inverted device structure for enhance both stability and PCE. The indium tin oxide (ITO) which has been used as anode can be applied as transparent cathode modified by n-type metal oxides, metal carbonates [16–22], cesium carbonate, conjugated polyelectrolyte [23–25], self-assembled cross-linked fullerene [26,27] and self-assembled polar molecules [28]. In addition, inverted PSCs which can fabricated with the high-work function and air-stable metals (ex: Ag, Au, etc.) as anode for enhancing a stability.

Otherwise, poly(3,4-ethylene dioxythiophene): poly(styrene sulfonate) (PEDOT:PSS) can be applied as an anode buffer layer in inverted PSCs. PEDOT:PSS has the

* Corresponding author. Tel.: +82 2 450 3498; fax: +82 2 444 0765.
E-mail address: dkmoon@konkuk.ac.kr (D.K. Moon).

1566-1199/$ - see front matter © 2013 Elsevier B.V. All rights reserved.
http://dx.doi.org/10.1016/j.orgel.2013.03.036

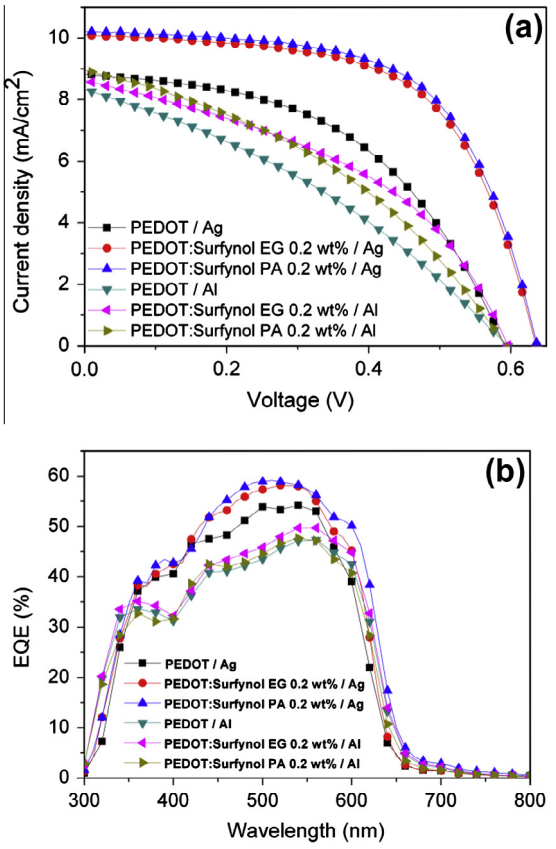

Fig. 1. (a) *J–V* characteristics and (b) external quantum efficiency (EQE) characteristics of the inverted PSCs based on P3HT:PCBM = 1:0.6 blend films with different anode buffer layers.

following advantages; high work function, high transparency and good conductivity. In conventional PSCs, however, long-term stability decreased after ITO was corroded by the strong acid 'PSS' in PEDOT:PSS [29]. Because of hydrophilic characteristics of PEDOT:PSS, in addition, inconstant film morphology and electrical property were observed when it deposited on the hydrophobic polymer blend layer in inverted PSC [30,31].

To solve this kind of problem, inorganic materials such as V_2O_5 [16], WO_3 [32], NiO [33] and MoO_3 [34] were investigated to replace PEDOT:PSS. However, they require complicated processes such as deposition through the expensive thermal evaporation process, synthesis of precursor solution, hydrothermal processing or calcinations required to induce crystallization.

In this study, therefore, we introduced a modified PEDOT:PSS in inverted PSCs as a anode buffer layer for solution process. To deposit hydrophilic PEDOT:PSS on the hydrophobic polymer blend layer with a homogeneous film, the amphiphilic surfactant 'Sufynol 104 series' was added to the PEDOT:PSS. The performance of the inverted PSCs with various anode and amphiphilic surfactant were evaluated and the stability of devices was measured.

2. Materials and measurements

2.1. Materials

The indium tin oxide (ITO) glass that was used as the transparent electrode is a Samsung Corning product (ITO: 170 nm, 10 Ω/sq). Poly(3,4-ethylenedioxythiophene)/poly(styrenesulfonate) (PEDOT:PSS, AI 4083) was purchased from Clevios and P3HT, which was used as a donor material in the photoactive layer, was purchased from Rieke metal. PCBM, the acceptor material, was purchased from Nano C. ZnO precursor was synthesized in accordance with the method mentioned in the literature [35]. The Surfynol 104 EG (Surfynol dissolve in ethylene glycol at 50 wt.%) and Sufynol 104 PA (Surfynol dissolve in isopropyl alcohol at 50 wt.%), which was used as an amphiphilic surfactant, was purchased from AirProduct. The chemical structures of P3HT, PCBM and Surfynol 104 are shown in Fig. 4b.

2.2. Measurements

All of the thin films were fabricated using a GMC2 spin coater (Gensys), and their thicknesses were measured using an alpha step 500 surface profiler (KLA-Tencor). The morphology of the anode buffer layers was observed through atomic force microscopy (AFM, PSIA XE-100) and energy-filtered transmission electron microscopy (EFTEM, Carl Zeiss AG LIBRA 120).The surface energy was measured with a contact-angle meter (KRUSS K6). The Raman spectroscopy measurement was performed using T64000 (HORIABA Jobin Yvon). The current density–voltage (*J–V*) characteristics of the PSCs were measured using a Keithley

Table 1
Photovoltaic performances in solution processable inverted PSCs composed P3HT:PCBM fabricated with various surfactants added PEDOT:PSS layer and metal electrodes.

Electrode	Surfactant	J_{SC} (mA/cm^2)	V_{OC} (V)	FF (%)	PCE (%)	R_S (Ω cm^2)	R_{SH} (Ω cm^2)
Ag	None	8.8	0.59	48.4	2.5	20.0	604
Al	None	8.1	0.59	33.7	1.6	42.2	142
Ag	Surfynol PA (0.2 wt.%)	10.2	0.63	61.3	4.0	10.8	1424
	Surfynol EG (0.2 wt.%)	10.1	0.63	60.3	3.8	11.3	1349
Al	Surfynol PA (0.2 wt.%)	8.7	0.59	42.6	2.2	31.4	189
	Surfynol EG (0.2 wt.%)	9.0	0.59	37.7	2.0	20.4	174

ITO (170 nm)/ZnO (30 nm)/P3HT:PCBM (1:0.6)/PEDOT:PSS *w/w.o* surfactant (40 nm)/Al or Ag (100 nm).

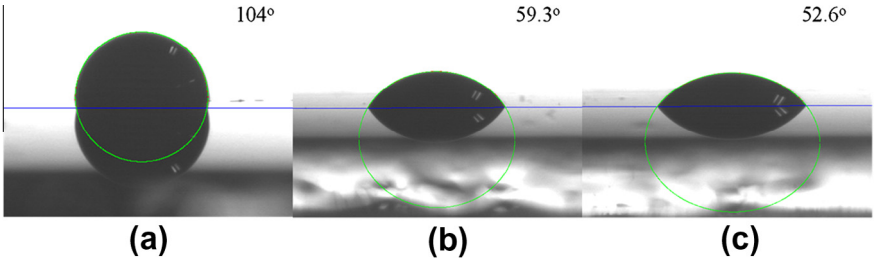

Fig. 2. Pictures of a drop of (a) pristine PEDOT:PSS, (b) Surfynol 104 EG and (c) Surfynol 104 PA doped PEDOT:PSS on the surface of P3HT:PCBM film.

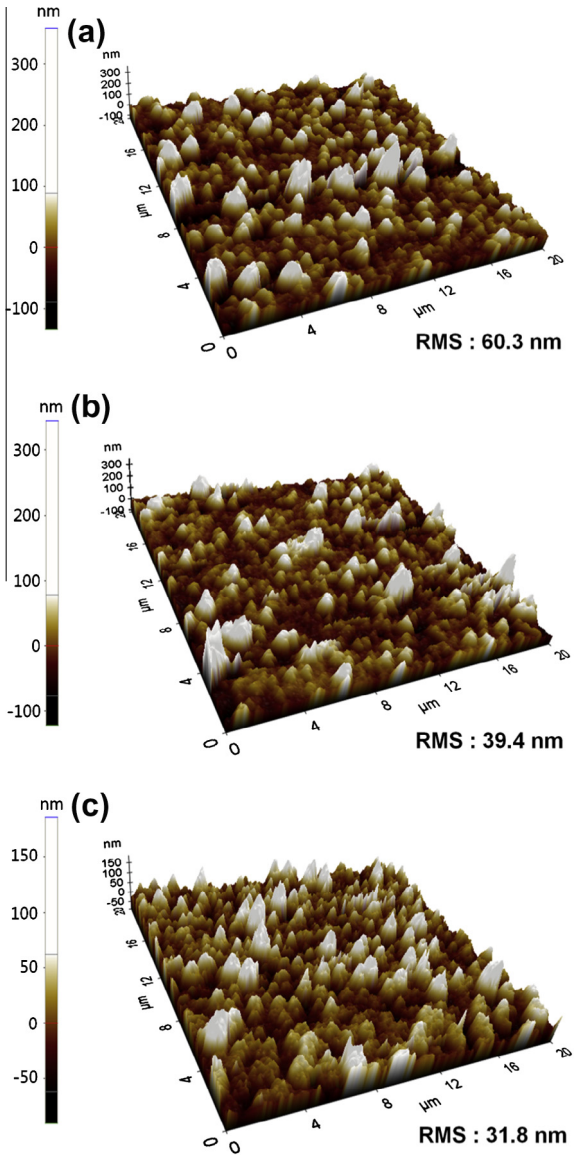

Fig. 3. AFM images of the surfaces form (a) pristine PEDOT:PSS/P3HT:PCBM, (b) Surfynol 104 EG doped PEDOT:PSS/P3HT:PCBM and (c) Surfynol 104 PA doped PEDOT:PSS/P3HT:PCBM.

2400 source measure unit. The devices were evaluated at 298 K by using a Class A Oriel solar simulator (Oriel 96,000 150 W solar simulator) having an xenon lamp that simulates AM 1.5G irradiation (100 mw/cm^2) from 400 to 1100 nm. The instrument was calibrated with a monocrystalline Si diode fitted with a KG5 filter to bring the spectral mismatch to unity. The calibration standard was calibrated by the National Renewable Energy Laboratory (NREL). IPCE (Mc science) was measured against the best performance device.

3. Experimental

3.1. Cleaning of patterned ITO glass

To clean the patterned ITO glass, it was sonicated for 20 min. in each of detergent (Alconox® in deionized water, 10%), acetone, isopropyl alcohol and deionized water in order. The moisture was removed by blowing thoroughly with N_2 gas. To ensure complete removal of all of the remaining water, the patterned ITO glass was baked on a hot plate for 10 min at 100 °C. For hydrophilic treatment of the patterned ITO glass, it was cleaned for 10 min in a UVO cleaner.

3.2. Fabrication of PSCs

ZnO precursor was spin coated aqueous solution to form a 30 nm thick film on the patterned ITO glass. The substrate was dried for 60 min at 90 °C in air and then transferred into a glovebox to spin coat the active layer. A solution containing a mixture of P3HT/PCBM (1:0.6) in ODCB was then spin coated on top of the ZnO layer to give a 130-nm-thick photoactive layer that was then thermal annealing at 160 °C for 10 min. To form a anode buffer layer, the Surfynol 104 EG and Surfynol 104 PA were dissolved in PEDOT:PSS at a various concentrations from 0.1 wt.% to 0.3 wt.%. The solution was then spin coated onto the photo active layer to form a 40 nm-thick layer and then annealed at 120 °C for 20 min. To form the metal cathode, Al (5 Å/s, 100 nm) was thermally deposited in a high-vacuum (<10^{-7} torr) chamber.

4. Results and discussion

Fig. 1 shows *J–V* curve and IPCE data when Surfynol 104 EG and Surfynol 104 PA were added to PEDOT:PSS as surfactants with Al and Ag as anodes. The results were stated in Table 1. The PCE of PSC with Ag anode was higher than PSC with Al anode. In general, Ag is 4.3 eV in terms of work

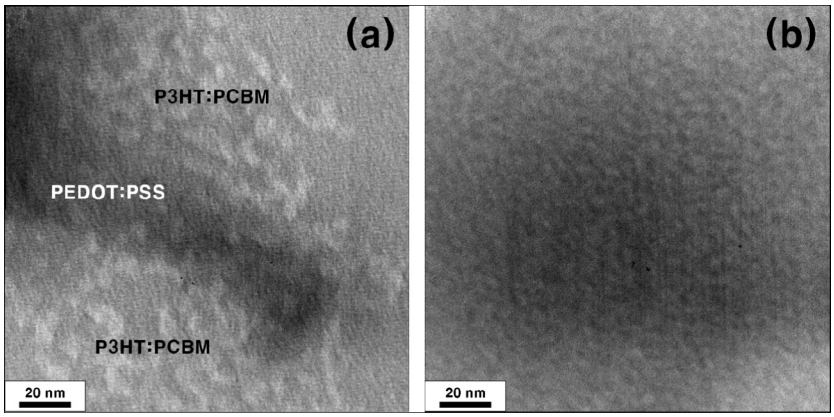

Fig. 4. EF-TEM images of the surface morphology (a) pristine PEDOT:PSS/P3HT:PCBM, (b) Surfynol 104 PA doped PEDOT:PSS/P3HT:PCBM.

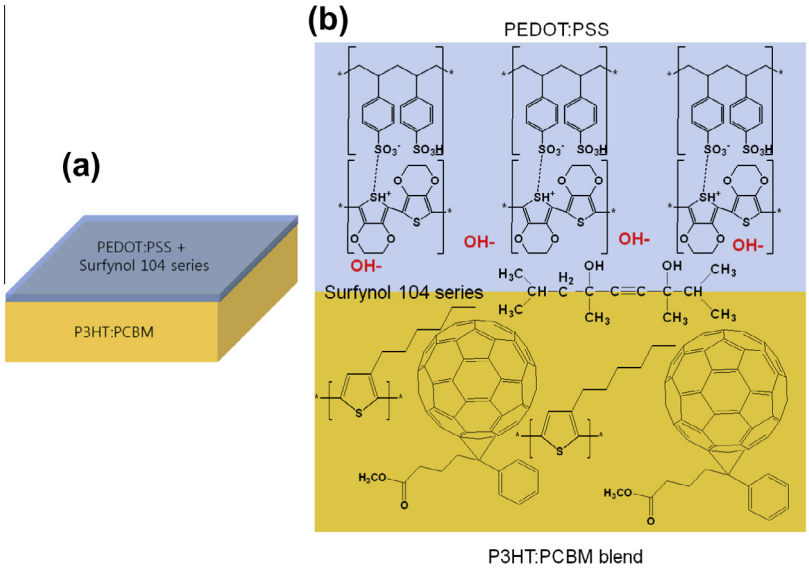

Fig. 5. (a) Structure of Surfynol 104 series doped PEDOT:PSS/P3HT:PCBM and (b) schematic depiction of the role of the Surfynol 104 series in the solution of PEDOT:PSS and P3HT:PCBM interface.

function. However, the work function increases to 5.0 eV through oxidization in the air. Therefore, it can collect holes which are dissociated from donor materials such as P3HT more effectively [36].

When Surfynol 104 EG and Surfynol 104 PA were added to PEDOT:PSS at 0.2 wt.%, respectively, the device performance was optimized. When Ag was applied as anode, PCE was 3.8% and 4.0% respectively (the optimization data of devices are shown in Supporting information Figs. S1 and S2). This result was improved about 60% compared to the reference device (2.5% of PCE) which was applied pristine PEDOT:PSS as an anode buffer layer. The important thing is that short circuit current density (J_{SC}) and fill factor (FF) significantly increased after adding Surfynol 104 series to PEDOT:PSS. The reference device with Ag anode was 8.8 mA/cm^2 in terms of J_{SC}. However, the J_{SC} were increased to 10.2 and 10.1 mA/cm^2 respectively in surfactant-added devices. In terms of FF, moreover, the reference device was 48.4%. However, the FF increased to 61.3% and 60.3% respectively in Surfynol 104 series-added devices. When PEDOT:PSS was applied as an anode buffer layer, the results were different from the previous studies in which reducing device current efficiency was observed [30,31,37]. Therefore, it was expected that the characteristics of the anode buffer layer changed with the addition of Surfynol 104 series to PEDOT:PSS. For analysis of this change, various surface analyses were conducted.

Fig. 2 shows pictures of a drop of pristine PEDOT:PSS and Surfynol 104 PA doped PEDOT:PSS on the surface of P3HT:PCBM film. The contact angle was decreased from 104° to 52.6° by Surfynol 104 PA added to PEDOT:PSS, which means that surface energy was changed due to the effect of surfactant. Therefore, it has been confirmed that the hydrophobic P3HT:PCBM surface became hydrophilic

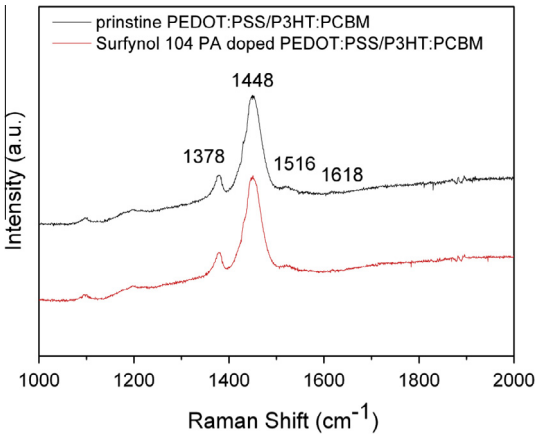

Fig. 6. Raman spectra of pristine PEDOT:PSS/P3HT:PCBM and Surfynol 104 PA doped PEDOT:PSS/P3HT:PCBM.

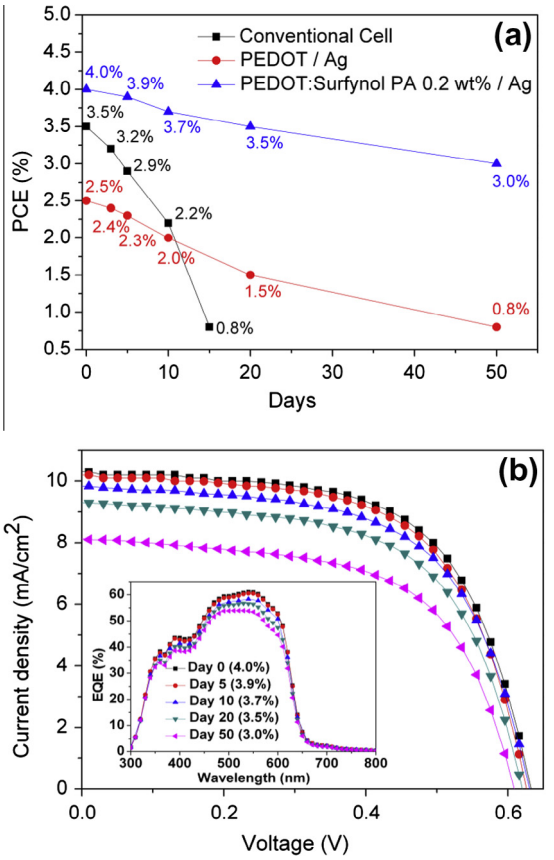

Fig. 7. (a) PCE as a function of storage time for P3HT:PCBM based inverted PSCs fabricated with PEDOT:PSS and Surfynol 104 PA doped PEDOT:PSS and conventional PSCs in air under ambient conditions (no encapsulation), (b) *J–V* curves as a storage time for P3HT:PCBM based inverted PSCs fabricated with Surfynol 104 PA doped PEDOT:PSS (inset: EQE data).

because of Surfynol 104 PA. To confirm the morphology of the anode buffer layer, surface analysis was conducted using AFM.

Fig. 3 shows the morphology images of the thin-films which are pristine PEDOT:PSS (Fig. 3a), Surfynol 104 EG doped PEDOT:PSS (Fig. 3b) and Surfynol 104 PA doped PEDOT:PSS (Fig. 3c) on the P3HT:PCBM film by AFM. In hydrophilic pristine PEDOT:PSS, rough root mean square (RMS) roughness (60.3 nm) was observed because of difference of surface energy with the hydrophobic P3HT:PCBM layer. In case of Surfynol series dopped PEDOT:PSS, however, roughness (Surfynol 104 EG: 39.4 nm, Surfynol 104 PA: 31.8 nm) decreased by more than 50% as the surface of the P3HT:PCBM film became hydrophilic. The morphologies of PEDOT:PSS with/without Surfynol 104 PA on active layer were further confirmed by the EFTEM (Fig. 4). EFTEM enables us to use 30 eV energy loss to distinguish PCBM domain, and provide more detailed morphology information than conventional TEM technique. Through this, we can be found that the bright domain is PCBM-rich domain [38]. As shown in Fig. 4b, Surfynol 104 PA doped PEDOT:PSS film could be obtained very uniform film.

As shown in Table 1, the shunt resistance (R_{SH}) of the pristine PEDOT:PSS-based reference device was 604 $\Omega\,cm^2$, but it increased to 1424 $\Omega\,cm^2$ in the Surfynol 104 PA-added devices. As a result, it has been confirmed that the surface morphology of buffer layer improved with an addition of surfactant, and FF increased by more than 24% with a reduction of charge recombination between the P3HT:PCBM layer and Ag interface [39]. In addition, increase in the surface morphology of buffer layer caused decrease in the internal resistance of devices. As a result, series resistance (R_S) was decreased from 20.0 to 10.8 $\Omega\,cm^2$. Therefore, J_{SC} was increased by more than 15% from 8.8 to 10.2 mA/cm^2 in the device in which the Surfynol 104 PA-added buffer layer was introduced as a buffer layer.

Fig. 5 shows the mechanism of forming a homogenous film on the hydrophobic P3HT:PCBM film by the Surfynol 104 series-doped PEDOT:PSS. Surfynol 104 series are an amphiphilic surfactant which consists of hydrophobic alkyl backbone and hydrophilic hydroxyl group. Hence, hydrophobic/hydrophobic interactions such as van der Waals interaction and other multiple weak interactions take place in the hydrophobic backbone of the Surfynol 104 series in PEDOT:PSS and hydrophobic P3HT:PCBM surface [40,41]. Therefore, the P3HT:PCBM surface became hydrophilic because of the hydroxyl group in the Surfynol 104 series. As a result, hydrophilic PEDOT:PSS can form a film on the P3HT:PCBM layer. In addition, the Surfynol 104 series are negatively charged in aqueous solution due to the hydroxyl groups. Therefore, during spin coating process of PEDOT:PSS which contains polycation PEDOT, there will be electrostatic interaction between the PEDOT and Surfynol 104 series. Thanks to these reasons, PEDOT:PSS was able to form a homogeneous film with improved wettability in the P3HT:PCBM layer (Fig. 5).

To study the structural properties of the anode buffer layer on P3HT:PCBM, the Raman spectra were measured for the pristine PEDOT:PSS/P3HT:PCBM, and the Surfynol 104 PA doped PEDOT:PSS/P3HT:PCBM, as shown in Fig. 6. The spectrum of the Surfynol 104 PA doped PEDOT:PSS/P3HT:PCBM was very similar to the corresponding

spectrum of the pristine PEDOT:PSS/P3HT:PCBM. From the Raman spectroscopy it was revealed that the Surfynol 104 PA was removed from PEDOT:PSS when the PEDOT:PSS annealed at 120 °C. Therefore, we confirmed that the conductivity of PEDOT:PSS does not decrease due to the surfactant in the presence of the PEDOT:PSS.

Fig. 7 shows the result of the air stability test on the inverted PSCs which introduced pristine PEDOT:PSS, Surfynol 104 PA-doped PEDOT:PSS and conventional PSC, which was performed for 50 days. In terms of the stability of unencapsulated PSCs, the device with Surfynol 104 PA doped PEDOT:PSS was the highest. About 25% of degradation was observed for 50 days. In the inverted PSC with pristine PEDOT:PSS, however, PCE decreased up to about 1/3 of the beginning during the same period. As expected, degradation rate was the fastest in the conventional PSC. Based on this result, it has been confirmed that the addition of Surfynol 104 series was changed the P3HT:PCBM layer from hydrophobic to hydrophilic and enhanced in-air stability.

5. Conclusions

In this study, solution processable inverted PSCs were fabricated by introducing surfactant doped PEDOT:PSS as an anode buffer layer for enhancing the stability and the PCE. Surfynol 104 series has amphiphilic characteristics, it supported the formation of a homogeneous anode buffer layer on the P3HT:PCBM film between the hydrophobic P3HT:PCBM film and hydrophilic PEDOT:PSS. Therefore, it was increased J_{SC} and FF to 10.2 mA/cm^2 and 61.3% respectively by reducing R_S and increasing R_{SH} in the inverted PSC. In addition, it was enhanced in-air stability.

Acknowledgement

This research was supported by a grant(10037195) from the Fundamental R&D Program for Core Technology of Materials funded by the Ministry of Knowledge Economy, Republic of Korea and the technology supporting project grant funded by the Korea government Ministry of Knowledge Economy (No.2012K10042360).

Appendix A. Supplementary material

Supplementary data associated with this article can be found, in the online version, at http://dx.doi.org/10.1016/j.orgel.2013.03.036.

References

[1] J.Y. Lee, Y.J. Kwon, J.W. Woo, D.K. Moon, Synthesis and characterization of fluorene–thiophene based π-conjugated polymers using coupling reaction, J. Ind. Eng. Chem. 14 (2008) 810–817.
[2] S.W. Heo, J.Y. Lee, H.J. Song, J.R. Ku, D.K. Moon, Patternable brush painting process for fabrication of flexible polymer solar cells, Sol. Energy Mater. Sol. Cells 95 (2011) 3041–3046.
[3] S.W. Heo, K.W. Song, M.H. Choi, T.H. Sung, D.K. Moon, Patternable solution process for fabrication of flexible polymer solar cells using PDMS, Sol. Energy Mater. Sol. Cells 95 (2011) 3564–3572.
[4] H.J. Song, D.H. Kim, E.J. Lee, S.W. Heo, J.Y. Lee, D.K. Moon, Conjugated polymer consisting of quinacridone and benzothiadiazole as donor materials for organic photovoltaics: coplanar property of polymer backbone, Macromolecules 45 (2012) 7815–7822.
[5] D.H. Yun, H.S. Yoo, S.W. Heo, H.J. Song, D.K. Moon, J.W. Woo, Y.S. Park, Synthesis and photovoltaic characterization of *D*/*A* structure compound based on *N*-substituted phenothiazine and benzothiadiazole, J. Ind. Eng. Chem. 19 (2013) 421–426.
[6] Z. He, C. Zhong, X. Huang, W.-Y. Wong, H. Wu, L. Chen, S. Su, Y. Cao, Simultaneous enhancement of open-circuit voltage, short-circuit current density, and fill factor in polymer solar cells, Adv. Mater. 23 (2011) 4636–4643.
[7] Z. He, C. Zhong, S. Su, M. Xu, H. Wu, Y. Cao, Enhanced power conversion efficiency in polymer solar cells using an inverted device structure, Nat. Photon. 6 (2012) 591–595.
[8] C.S. Kim, L.L. Tinker, B.F. DiSalle, E.D. Gomez, S. Lee, S. Bernhard, Y.L. Loo, Altering the thermodynamics of phase separation in inverted bulk hetero-junction organic solar cells, Adv. Mater. 21 (2009) 3110–3115.
[9] D.W. Zhao, L. Ke, Y. Li, S.T. Tan, A.K.K. Kyaw, H.V. Demir, X.W. Sun, D.L. Carroll, G.Q. Lo, D.L. Kwong, Optimization of inverted tandem organic solar cells, Sol. Energy Mater. Sol. Cells 95 (2011) 921–926.
[10] H. Ma, H.L. Yip, F. Huang, A.K.Y. Jen, Interface engineering for organic electronics, Adv. Funct. Mater. 20 (2010) 1371–1388.
[11] P.K. Sudeep, K.T. Early, K.D. McCarthy, M.Y. Odoi, M.D. Barnes, T. Emrick, Monodisperse oligo(phenylene vinylene) ligands on CdSe quantum dots: synthesis and polarization anisotropy measurements, J. Am. Chem. Soc. 130 (2008) 2384–2385.
[12] K.H. Tsai, J.S. Huang, M.Y. Liu, C.H. Chao, C.Y. Lee, S.C. Hung, C.F. Lin, High efficiency flexible polymer solar cells based on PET substrates with a nonannealing active layer, J. Electrochem. Soc. 156 (2009) B1188–B1191.
[13] A. Wicklein, S. Ghosh, M. Sommer, F. Wurthner, M. Thelakkat, Self assembly of semiconductor organogelator nanowires for photoinduced charge separation, ACS Nano 3 (2009) 1107–1114.
[14] M. Jorgensen, K. Norrman, F.C. Krebs, Stability/degradation of polymer solar cells, Sol. Energy Mater. Sol. Cells 92 (2008) 686–714.
[15] T. Oyamada, C. Maeda, H. Sasabe, C. Adachi, Efficient electron injection mechanism in organic light-emitting diodes using an ultra thin layer of low-work-function metals, Jpn. J. Appl. Phys. 42 (2003) L1535–L1538.
[16] G. Li, C.W. Chu, V. Shrotriya, J. Huang, Y. Yang, Efficient inverted polymer solar cells, Appl. Phys. Lett. 88 (2006) 253503-1–253503-3.
[17] C. Waldauf, M. Morana, P. Denk, P. Schilinsky, K. Coakley, S.A. Choulis, C.J. Brabec, Highly efficient inverted organic photovoltaics using solution based titanium oxide as electron selective contact, Appl. Phys. Lett. 89 (2006) 233517-1–233517-3.
[18] J. Huang, G. Li, Y. Yang, A semi-transparent plastic solar cell fabricated by a lamination process, Adv. Mater. 20 (2008) 415–419.
[19] T. Ameri, G. Dennler, C. Waldauf, H. Azimi, A. Seemann, K. Forberich, J. Hauch, M. Scharber, K. Hingerl, C.J. Brabec, Fabrication, optical modeling, and color characterization of semitransparent bulk-heterojunction organic solar cells in an inverted structure, Adv. Funct. Mater. 20 (2010) 1592–1598.
[20] T. Yang, W. Cai, D. Qin, E. Wang, L. Lan, X. Gong, J. Peng, Y. Cao, Solution-processed zinc oxide thin film as a buffer layer for polymer solar cells with an inverted device structure, J. Phys. Chem. C 114 (2010) 6849–6853.
[21] Y. Sun, J.H. Seo, C.J. Takacs, J. Seifter, A.J. Heeger, Inverted polymer solar cells integrated with a low-temperature-annealed sol–gel-derived ZnO film as an electron transport layer, Adv. Mater. 23 (2011) 1679–1683.
[22] C.E. Small, S. Chen, J. Subbiah, C.M. Amb, S.W. Tsang, T.H. Lai, J.R. Reynolds, F. So, High-efficiency inverted dithienogermole–thienopyrrolodione based polymer solar cells, Nat. Photon. 6 (2012) 115–120.
[23] S.I. Na, T.S. Kim, S.H. Oh, J. Kim, S.S. Kim, D.Y. Kim, Enhanced performance of inverted polymer solar cells with cathode interfacial tuning via water-soluble polyfluorenes, Appl. Phys. Lett. 97 (2010) 223305-1–223305-3.
[24] H. Choi, J.S. Park, E. Jeong, G.H. Kim, B.R. Lee, S.O. Kim, M.H. Song, H.Y. Woo, J.Y. Kim, Combination of titanium oxide and a conjugated polyelectrolyte for high-performance inverted-type organic optoelectronic devices, Adv. Mater. 23 (2011) 2759–2763.
[25] Y. Zhu, X. Xu, L. Zhang, J. Chen, Y. Cao, High efficiency inverted polymeric bulk-heterojunction solar cells with hydrophilic conjugated polymers as cathode interlayer on ITO, Sol. Energy Mater. Sol. Cells 97 (2012) 83–88.
[26] Y.J. Cheng, C.H. Hsieh, Y. He, C.S. Hsu, Y. Li, Combination of indene-C_{60} bis-adduct and cross-linked fullerene interlayer leading to highly

efficient inverted polymer solar cells, J. Am. Chem. Soc. 132 (2010) 17381–17383.
[27] C.H. Hsieh, Y.J. Cheng, P.J. Li, C.H. Chen, M. Dubosc, R.M. Liang, C.S. Hsu, Highly efficient and stable inverted polymer solar cells integrated with a cross-linked fullerene material as an interlayer, J. Am. Chem. Soc. 132 (2010) 4887–4893.
[28] J.S. Park, B.R. Lee, J.M. Lee, J.S. Kim, S.O. Kim, M.H. Song, Efficient hybrid organic-inorganic light emitting diodes with self-assembled dipole molecule deposited metal oxides, Appl. Phys. Lett. 96 (2010) 243306-1–243306-3.
[29] M.P. de Jong, L.J. van Ijzendoorn, M.J.A. de Voigt, Stability of the inter- face between indium-tin-oxide and poly(3,4-ethylenedioxythiophene)/poly(styrenesulfonate) in polymer light-emitting diodes, Appl. Phys. Lett. 77 (2000) 2255–2257.
[30] M. Kemerink, S. Timpanaro, M.M. Kok, E.A. Meulenkamp, F.-J. Touwslager, Three-dimensional inhomogeneities in PEDOT:PSS films, J. Phys. Chem. B 108 (2004) 18820–18825.
[31] C. Ionescu-Zanetti, A. Mechler, S.A. Mechler, R. Lal, Semiconductive polymer blends: correlating structure with transport properties at the nanoscale, Adv. Mater. 16 (2004) 385–389.
[32] C. Tao, S. Ruan, G. Xie, X. Kong, L. Shen, F. Meng, C. Liu, X. Zhang, W. Dong, W. Chen, Role of tungsten oxide in inverted polymer solar cells, Appl. Phys. Lett. 94 (2009) 043311-1–043311-3.
[33] K.X. Steirer, J.P. Chesin, N.E. Widjonarko, J.J. Berry, A. Miedaner, D.S. Ginley, D.C. Olson, Solution deposited NiO thin-films as hole transport layers in organic photovoltaics, Org. Electron. 11 (2010) 1414–1418.
[34] A.K.K. Kyaw, X.W. Sun, C.Y. Jiang, G.Q. Lo, D.W. Zhao, D.L. Kwong, An inverted organic solar cell employing a sol–gel derived ZnO electron selective layer and thermal evaporated MoO_3 hole selective layer, Appl. Phys. Lett. 93 (2008) 221107-1–221107-3.
[35] H. Li, J. Wang, H. Liu, C. Yang, H. Xu, X. Li, H. Cui, Sol–gel preparation of transparent zinc oxide films with highly preferential crystal orientation, Vacuum 77 (2004) 57–62.
[36] M.S. White, D.C. Olson, S.E. Shaheen, N. Kopidakis, D.S. Ginley, Inverted bulk-heterojunction organic photovoltaic device using a solution-derived ZnO underlayer, Appl. Phys. Lett. 89 (2006) 143517-1–143517-3.
[37] M.D. Irwin, D.B. Buchholz, A.W. Hains, R.P.H. Chang, T.J. Marks, P-type semiconducting nickel oxide as an efficiency-enhancing anode interfacial layer in polymer bulk-heterojunction solar cells, Proc. Natl. Acad. Sci. USA 105 (2008) 2783–2787.
[38] J. You, L. Dou, K. Yoshimura, T. Kato, K. Ohya, T. Moriarty, K. Emery, C.-C. Chen, J. Gao, G. Li, Y. Yang, A polymer tandem solar cell with 10.6% power conversion efficiency, Nat. Commun. 4 (2013) 1446, http://dx.doi.org/10.1038/ncomms2411.
[39] X. Yang, J. Loos, S.C. Veenstra, W.J.N. Verhees, M.M. Wienk, J.M. Kroon, M.A.J. Michels, R.A.J. Janssen, Nanoscale morphology of high-performance polymer solar cells, Nano Lett. 5 (2005) 579–583.
[40] L. Wang, X. Wang, M.F. Xu, D.D. Chen, J.Q. Sun, Layer-by-layer assembled microgel films with high loading capacity: reversible loading and release of dyes and nanoparticles, Langmuir 24 (2008) 1902–1909.
[41] S.K. Hau, H.L. Yip, N.S. Baek, J.Y. Zou, K. O'Malley, A.K.Y. Jen, Air-stable inverted flexible polymer solar cells using zinc oxide nanoparticles as an electron selective layer, Appl. Phys. Lett. 92 (2008) 253301-1–253301-3.